High temperature compression of Mo(Si,Al)2-Al2O3 composites

Citation for the original published paper (version of record):
Edgren, A., Ström, E., Frisk, L. et al (2023). High temperature compression of Mo(Si,Al)2-Al2O3 composites. Materials Science & Engineering A: Structural Materials: Properties, Microstructure and Processing, 865. http://dx.doi.org/10.1016/j.msea.2023.144583

Materials Science & Engineering A 865 (2023) 144583

Contents lists available at ScienceDirect

Materials Science & Engineering A

journal homepage: www.elsevier.com/locate/msea

High temperature compression of $Mo(Si,Al)_2$-Al_2O_3 composites

Aina Edgren [a,b], Erik Ström [b], Lars Frisk [c], Farid Akhtar [c], Magnus Hörnqvist Colliander [a,*]

[a] Chalmers University of Technology, Gothenburg, SE-41296, Sweden
[b] Kanthal AB, Hallstahammar, SE-73427, Sweden
[c] Luleå University of Technology, Luleå, SE-97187, Sweden

ARTICLE INFO

Keywords:
$Mo(si,Al)_2$
Particle strengthening
High temperature compression
Electron backscatter diffraction
Electroplasticity

ABSTRACT

The aim of this study was to investigate the effect on high temperature of mechanical properties of adding Al_2O_3 particles to polycrystalline $Mo(Si,Al)_2$. $Mo(Si,Al)_2$-Al_2O_3 composites, containing 0–25 wt% Al_2O_3 particles have been compression tested at 1300 °C, and the microstructure after deformation was studied using electron backscatter diffraction. It was shown that even small amounts (5 wt%) of Al_2O_3 particles resulted in a grain-refined material through inhibition of grain growth during sintering, which lead to lower flow stresses compared to the coarse-grained Al_2O_3-free material. The inverse grain size effect and post-test microstructure investigations suggest that creep-like deformation mechanisms dominate in fine grained $Mo(Si,Al)_2$-Al_2O_3 composites at 1300 °C. In the materials containing 5–15 wt% Al_2O_3, the maximum stress decreased with increasing Al_2O_3 content. In materials with higher Al_2O_3 additions, the maximum stress increased with the Al_2O_3 addition, but did not reach the strength levels in the Al_2O_3-free reference material. It is suggested that the deformation behaviour is affected by electroplasticity effects as resistive heating was used. Electroplasticity contributes to the decrease in maximum stress observed in the lower Al_2O_3 containing materials, while this is outweighed by particle strengthening at higher Al_2O_3 contents.

1. Introduction

High temperature heating processes (above 1000 °C), for example within the steel industry, give rise to significant greenhouse gas emissions [1]. Most of the energy used for the processes is produced through combustion of fossil fuels [2], and their electrification therefore holds a great promise to reduce the greenhouse gas emission. Electric alternatives, for example indirect resistive heating using heating elements, are already used in small furnaces, operating at high temperature. Resistive heating is a mature technology with high potential also for larger industrial furnaces, operating in the MW rather than in the kW range. However, this requires an up-scaling of the size of the heating elements and probably a more complicated mounting geometry (horizontal rather than vertical) of the elements in the furnace. This will increase the demands on the mechanical properties of the heating elements since the gravitational force on them increases.

The choice of heating element material depends on the required temperature and operating environment. A material often used for high temperature heating elements in small furnaces is $Mo(Si,Al)_2$. It is a ceramic material with high melting temperature, high resistivity and excellent corrosion resistance in both oxidizing and reducing environments [3]. The latter makes it a suitable material choice for many industrial heating processes. While the oxidation properties of $Mo(Si,Al)_2$ have been thoroughly investigated [4–10], research on high temperature mechanical properties of polycrystalline $Mo(Si,Al)_2$ is scarce. Instead, most current knowledge is derived from tests of single crystals. It has been shown that $Mo(Si,Al)_2$, which possesses a hexagonal crystal structure (Strukturbericht Designation C40), only has one possible slip system, $\langle 2\bar{1}\bar{1}0\rangle(0001)$, which is activated above 1100 °C [11]. However, due of the complex stress state and the influence of grain boundaries, the deformation mechanisms in polycrystalline materials are expected to be more complicated than in single crystals.

When it comes to polycrystalline C40-structured $Mo(Si,Al)_2$ very few studies have been reported. Hagihara et al. [12] and Umakoshi et al. [13] studied the temperature dependence on yield strength and fracture strength at elevated temperature (800–1600 °C). A ductile–brittle transition temperature (DBTT) of 1250 °C was reported. The strength levels were similar to $C11_b$-structured $MoSi_2$ and fracture strains exceeding 20% were observed above the DBTT [12,13]. However, no complete stress–strain curves were presented. Niihara et al. [14] and Suzuki et al. [15] have studied the flexural strength of nanostructured $Mo(Si,Al)_2$ at temperatures up to 1300 °C. Common for the studies is that the microstructures after deformation were not investigated.

* Corresponding author.
E-mail address: magnus.colliander@chalmers.se (M. Hörnqvist Colliander).

https://doi.org/10.1016/j.msea.2023.144583
Received 21 October 2022; Received in revised form 15 December 2022; Accepted 2 January 2023
Available online 6 January 2023

In our previous study of polycrystalline $Mo(Si,Al)_2$ tested in compression at 1300 °C, we showed that a rapid softening took place after yielding [16]. We observed large variations in crystal orientations within the grains, which suggests that intragranular deformation through dislocation slip was an active deformation mechanism. The formation and movement of dislocations also gave rise to formation of low angle grain boundaries (LAGBs) within the grains. Furthermore, dynamic recrystallization (DRX), driven by the stored energy (dislocation density), took place during deformation.

It is suggested that particle strengthening could be used to improve the mechanical properties of $Mo(Si,Al)_2$. The particles are expected to pin the grain boundaries during sintering, which gives rise to a more fine-grained material [17–20]. A smaller grain size would, according to the Hall–Petch relationship, improve the strength of the material. On the other hand, a reduction in grain size has been shown to promote grain boundary sliding in other disilicides, but it has also been reported that addition of hard particles could suppress such sliding [18,21]. While $C11_b$-structured $MoSi_2$ has been the most extensively studied silicide-based material with respect to particle strengthening [14,15,17–19,22–24], Niihara et al. [14] and Suzuki et al. [15] have tested the flexural strength (three point bending test, from room temperature up to 1300 °C) of a $Mo(Si,Al)_2$-SiC nanocomposite. The chemical composition of the matrix phase was $Mo_{34.2}Si_{57.4}Al_{8.5}$ (lower Al content compared to the material investigated in our present, and previous study [16]) and consisted of both $C11_b$ (84.9 vol.%) and C40 (15.1 vol.%). It was shown that the flexural strength was somewhat higher than that of a SiC-free $Mo_{34.2}Si_{57.4}Al_{8.5}$ nanomaterial. The microstructure of the deformed material was not presented. However, no studies have been conducted in the case of a non-nanostructured C40 $Mo(Si,Al)_2$, even though particle strengthening has been used with success in other silicides.

In this study we investigate the effect of Al_2O_3 additions on the high temperature mechanical properties of C40 $Mo(Si,Al)_2$. Al_2O_3 was selected because Al is already present in the material and will not affect the oxidation behaviour. Compression tests were performed at 1300 °C using a Gleeble thermomechanical simulator. The test specimens were heated by resistive heating. We show that Al_2O_3 additions lead to more fine-grained materials, in which no DRX or formation of LAGBs occur during compression. The strength of the fine-grained Al_2O_3 containing materials was lower than that of a coarse-grained Al_2O_3-free reference, suggesting that creep-like deformation mechanisms, such as grain boundary sliding, dominate. For materials containing 5–15 wt% added Al_2O_3, the maximum stress decreases with increased Al_2O_3 content. We suggest this could be related to electroplasticity. At higher volume fractions, the particle strengthening outweighs the strength reduction due to electroplasticity.

2. Materials and methods

2.1. Materials

Polycrystalline $Mo(Si,Al)_2$ was prepared by dry mixing of elemental Mo (99.9% purity, Cerac Inc.), Si (99.99% purity, Wacker) and Al (99.5% purity, GoodFellow) powders in a Mo-lined ball mill with Mo balls. The powder mixture was heated in inert gas to initiate a self-propagating reaction in which $Mo(Si,Al)_2$ (as well as small amounts of $Mo_5(Si,Al)_3$ and Al_2O_3) was formed. $Mo_5(Si,Al)_3$ is formed as a result of local variations in the unreacted Mo-Si-Al powder. According to [25], an Al-Si eutectic forms when the powder is heated. This leads to regions with lower Si and Al content, which promotes the formation of $Mo_5(Si,Al)_3$, rather than $Mo(Si,Al)_2$. Furthermore, Al is consumed by the formation of Al_2O_3 during the reaction, which further lowers the Al content of the unreacted powder. The reaction product was milled in ball mill for 228 h to obtain a fine-grained powder with an average particle size of around 5 μm. Five $Mo(Si,Al)_2$-Al_2O_3 composites, containing 5, 10, 15, 20 and 25 wt% Al_2O_3 respectively, were prepared by adding Al_2O_3 particles (AKP-53, Sumitomo Chemical, purity: 99.99%, mean particle size: 0.17 μm), to the milled $Mo(Si,Al)_2$ powder, see Table 1. The powders were milled for 1 min in a vibratory disc mill to prevent agglomeration of Al_2O_3 particles. A reference material, without added Al_2O_3, was also prepared. The powders were compacted to rods using cold isostatic pressing (CIP, EPSI) operating at 2000 bar, prior sintering for 1 h at 1650 °C in H_2 gas in a tube furnace (ramp time from room temperature was 5 h). The as-sintered materials had densities of 97%–98%, of the theoretical values, see Table 1.

Table 1
Materials and theoretical density of materials.

	Reacted $Mo(Si,Al)_2$ powder (wt%)	Al_2O_3 (wt%)	Theoretical density (g/cm^3)
A0	100	0	6.01
A5	95	5	5.86
A10	90	10	5.72
A15	85	15	5.59
A20	80	20	5.46
A25	75	25	5.34

2.2. Materials characterization

An FEI Quanta 200 FEG ESEM scanning electron microscope (SEM) was used for microstructure imaging and chemical composition analysis using energy-dispersive X-ray spectroscopy (EDS). An acceleration voltage of 20 kV was used. Electron backscatter diffraction (EBSD) was used to obtain crystal orientation and grain size data. A Tescan Gaia 3 SEM, operating at 15 kV, was used for this purpose. The EBSD data were analysed in MTEX [26], and the grain size was calculated as the equivalent sphere diameter, $d = 2\sqrt{A/\pi}$, where A is the grain area. Grain reference orientation (GROD) maps were used to quantify the internal misorientations within grains, which is related to the density of geometrically necessary dislocations (GNDs). X-ray diffraction (XRD), using a Cu-anode equipped Bruker D8 Advance, was, along with EBSD, used for phase identification.

2.3. Compression testing

The as-sintered $Mo(Si,Al)_2$-Al_2O_3 composite rods were ground to a diameter of 8 mm and cut into 12 mm long cylindrical specimens for compression testing. The specimens were tested with a strain rate of 10^{-4} s^{-1} at 1300 °C using a Gleeble 3800 thermomechanical simulator. The temperature was measured using a pyrometer. Graphite foils and Ni-paste were used between the specimen and the anvils to minimize friction and ensure good electrical contact. More complete details and calibration of the experimental set-up are published elsewhere [16]. At least three specimens of each composite were tested.

3. Results

The mechanical properties and microstructure of the Al_2O_3-free material, A0, has been investigated in a previous paper [16], therefore, the results from this material will only be described in brief in this present paper.

3.1. Microstructure of as-sintered material

Backscattered electron (BSE) micrographs and EBSD phase maps of the as-sintered materials are shown in Fig. 1. All as-sintered materials consisted of three phases: $Mo(Si,Al)_2$, $Mo_5(Si,Al)_3$ and α-Al_2O_3. The chemical composition of the phases in A0 can be seen in Table 2. The composition of phases in the other materials are similar to those in A0. Since small amounts of Al_2O_3 was formed in the self-propagating reaction, also A0 contains Al_2O_3 (1.7 vol.%). The EBSD maps in Figs. 1

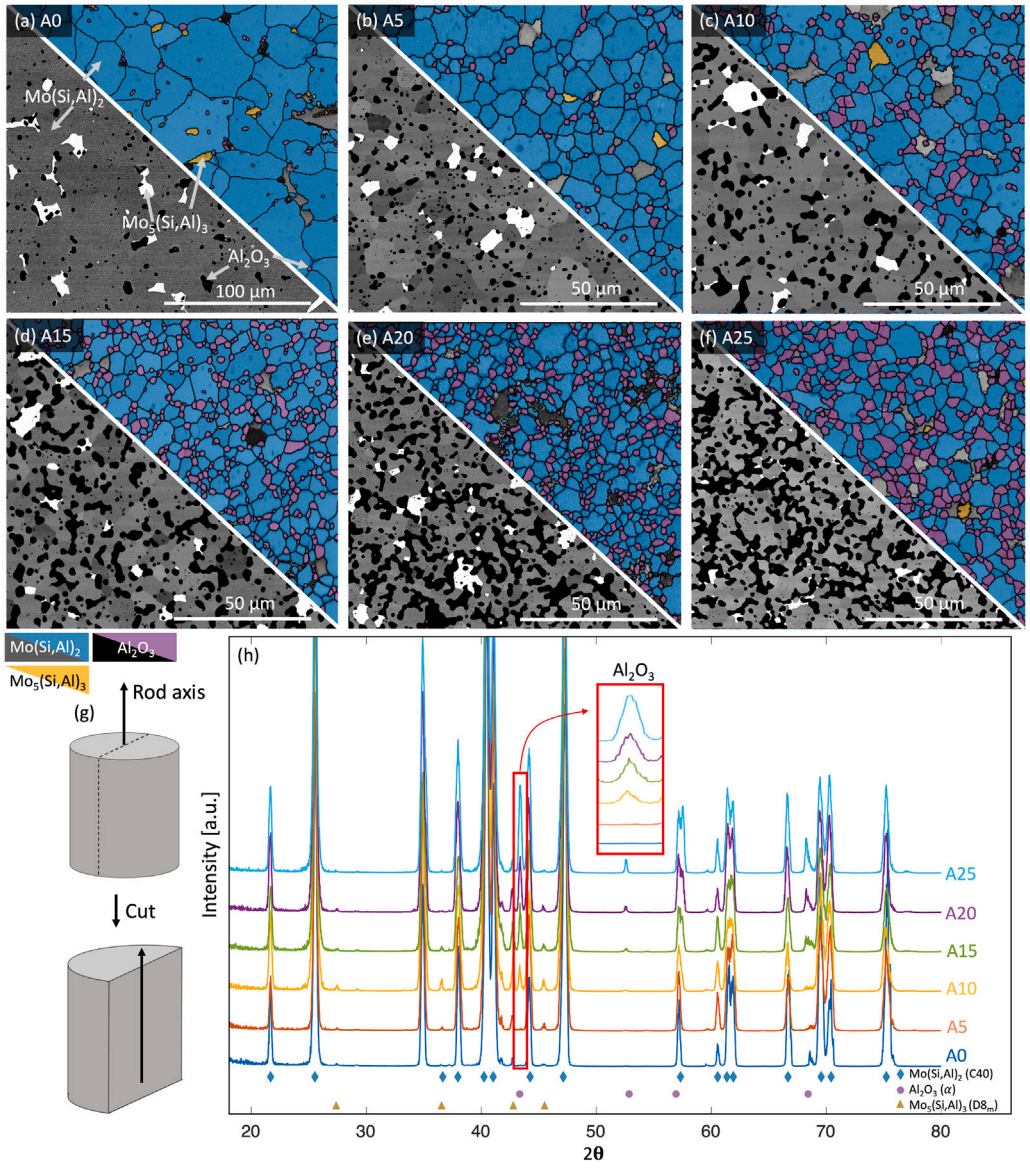

Fig. 1. BSE micrographs and EBSD phase maps of as-sintered materials, (a) A0, (b) A5, (c) A10, (d) A15, (e) A20, (f) A25, (g) cut of rod for microscopy study, (h) XRD diffractogram of A0-A25.

Table 2
EDS results on the chemical composition of the phases in A0.

Phase	Chemical composition [at.%]			
	Mo	Si	Al	O
$Mo(Si,Al)_2$	32.4	36.6	28.8	2.3
$Mo_5(Si,Al)_3$	57.2	32.6	7.3	2.8
Al_2O_3	0.8	1.7	39.6	58.0

and 2 shows that the grain size is much finer in A5-A25 (around 5 µm) compared with A0 (around 21 µm), see Table 3. This indicates that the addition of Al_2O_3 particles have a grain boundary pinning effect during sintering, which is in line with previous research on other disilicide composites [18,27]. The grain sizes are similar to the as-milled powder, and there is only a very slight decrease in grain size with increasing Al_2O_3 content (Table 3), suggesting that already the lowest levels of additions are sufficient to effectively pin the boundaries.

The Al_2O_3 particles in A5-A25 are larger (but typically less than 5 µm) than those formed from the self-propagating reaction (from nm up to 2–3 µm in size), compare Fig. 1(a) and (b)–(f), and located at $Mo(Si,Al)_2$ grain boundaries. The grey regions in the EBSD maps are unindexed $Mo(Si,Al)_2$ (some orientations are difficult to index even though the EBSD patterns were clear and belonged to a hexagonal unit cell) and $Mo_5(Si,Al)_3$ grains. The chemical composition of the unindexed grains agreed with $Mo(Si,Al)_2$ and $Mo_5(Si,Al)_3$, respectively. The low volume fraction of $Mo_5(Si,Al)_3$ in A0-A25 is not expected to affect the mechanical properties of the composites to a great extent. Furthermore, if there is an affect, it should be similar in all materials presented in this paper because of the similar volume fractions. Therefore, the EBSD analysis presented in this paper is limited to the $Mo(Si,Al)_2$ phase only. The amount of porosity is low and similar in all materials and should not have a major effect on the strength. Furthermore, in particular as the samples are tested in compression.

The chemical composition of the phases is shown in Table 2. The O content in $Mo(Si,Al)_2$ and $Mo_5(Si,Al)_3$ is likely due to the presence of nano-sized Al_2O_3 particles dispersed in the two phases. Such particles have been found in our previous study of the A0 material [16] using SEM and transmission electron microscopy (TEM), and have been reported in studies on a similar material by Ingemarsson et al. [4,6,7]. The unstoichiometric composition of Al_2O_3 and the detection of Mo and

Table 3
Volume fractions, grain size and density (as percent of theoretical density) for the different materials.

	Volume fraction [%]				$MoL(Si,Al)_2$ Grain size µm (std)	% of theoretical density
	$Mo(Si,Al)_2$	$Mo_5(Si,Al)_3$	Al_2O_3	Pores		
A0	94.2	3	1.7	1.1	21.41 (13.41)	95.3
A5	86.8	5.3	7.8	0.1	7.05 (3.30)	96.9
A10	81.1	4.7	14.1	0.1	5.12 (3.19)	97.9
A15	76.2	3.9	19.7	0.2	4.81 (2.41)	97.9
A20	67.8	3.7	26.9	1.5	3.80 (1.74)	97.7
A25	64.8	2.4	31.2	1.7	5.45 (2.21)	97.0

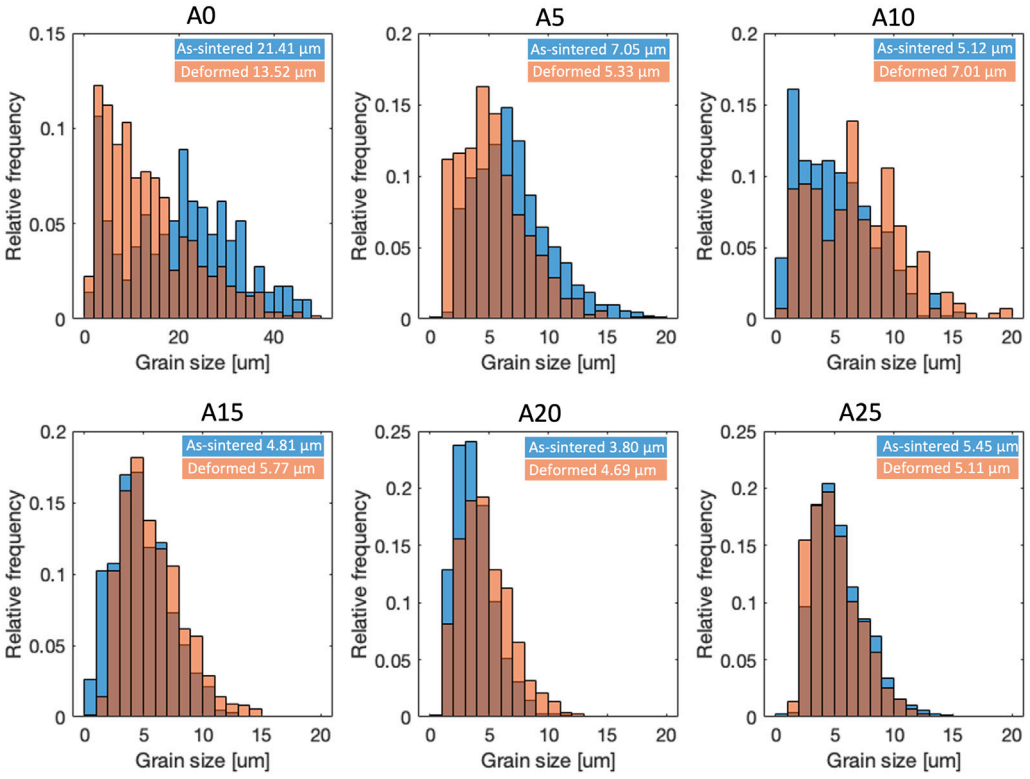

Fig. 2. Grain size distribution of as-sintered and deformed materials. Average grain size in legends.

Si in this phase is probably due to large interaction volume in SEM, and/or Mo and Si traces remaining from the synthesis.

3.2. Deformation behaviour

All specimens were plastically deformed when tested in compression at 1300 °C. Stress–strain curves of all material are shown in Fig. 3. The final strain differ between the specimens as a consequence of the experiment design, which was designed to include only the peak stress and the subsequent softening. The compression was manually stopped when the stress reached low values, typically between 20 and 40 MPa. The stress–strain curves from all specimens are found in supplementary materials. Some of the curves in this figure showed abrupt stress drops and lower maximum stress (for example the curves labelled A5.2, A10.3 and A15.4 in Fig. S1) than other specimens of the same material. The drops are probably related to defects, such as pores or flaws, present in the materials. The specimens giving rise to such curves were not selected for further investigations.

In the initial part of the deformation, all tested specimen showed linear behaviour before plastic deformation begins. After reaching the maximum stress, the materials soften rapidly. The details of the stress–strain curve obtained from A0 has been reported in [16], and here we focus on samples A5-A25. Compared with A0, the stress–strain curves of the Al_2O_3-added materials deviate from linearity at lower

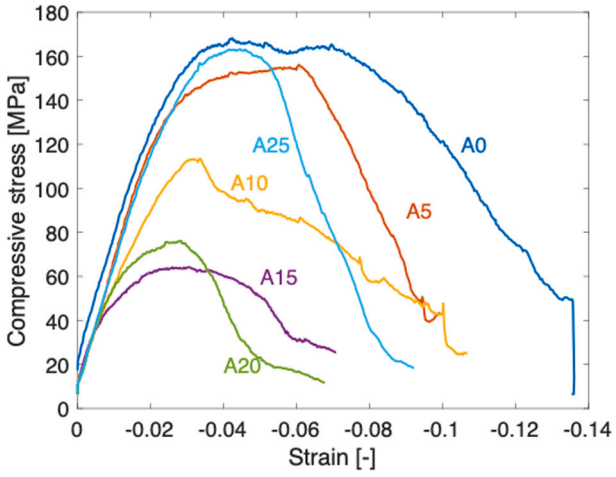

Fig. 3. Engineering stress–strain curves of selected specimens, corresponding to coloured markers in Fig. 4. (For interpretation of the references to colour in this figure legend, the reader is referred to the web version of this article.)

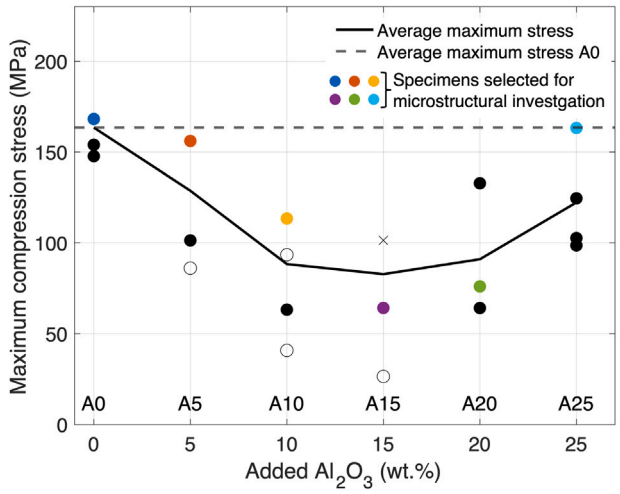

Fig. 4. Maximum stresses of all tested specimens. Open circles indicate specimens with abrupt stress drops. Filled circles indicate tests without stress drops, and the colours correspond to stress–strain curves in Fig. 3 (curves for black circles are shown in the supplementary material). The solid black line connects the average maximum stresses of the Al_2O_3-added materials, and the horizontal dashed line is a reference showing the average maximum stress of A0. The A15 specimen indicated by a cross fractured after deformation. (For interpretation of the references to colour in this figure legend, the reader is referred to the web version of this article.)

stress levels and the maximum stresses of the Al_2O_3-added materials are lower. This decrease in flow stress deviates from the grain size-strength relationship described by the Hall–Petch relationship. This indicates that a large grain boundary area is deleterious for the strength of polycrystalline $Mo(Si,Al)_2$. This in turn, indicates that the materials deform by creep-like mechanisms at 1300 °C.

The maximum stresses obtained from the compression tested specimens as a function of Al_2O_3 content are shown in Fig. 4. While the scatter in the A0 data was relatively small, all Al_2O_3-added materials showed larger scatter. Despite the scatter, a "U"-shaped trend of the maximum stress can be observed. In the case of A5-A15, the maximum stress decreases as the Al_2O_3 content increases, while it increases as the Al_2O_3 content is further increased.

3.3. Microstructure of deformed specimens

The specimen corresponding to the stress–strain curves in Fig. 3 were selected for microstructure investigations. The specimens were cut parallel to the compression axis, and prepared for EBSD as described in Section 2.2.

The EBSD investigation of the deformed specimens indicated that the deformation mechanisms differed between A0 and the Al_2O_3-added materials. However, all Al_2O_3-added materials had very similar microstructures. As presented in [16], the microstructure of the deformed A0 specimens showed clear signs of DRX, indicated by a shift in grain size distribution towards smaller grain sizes after deformation, as can be seen in Fig. 2(a). No such decrease was observed in any of the Al_2O_3-added materials, see Fig. 2(b)–(f). Hence, the softening of polycrystalline $Mo(Si,Al)_2$ cannot be explained by DRX solely.

In [16] it was also shown that low angle grain boundaries (LAGBs) formed during compression testing of $Mo(Si,Al)_2$, which probably contributed to the observed softening through recovery. In Fig. 5(a) a grain reference orientation deviation (GROD) map of this material is shown, and a number of LAGBs are indicated by arrows. In the Al_2O_3-added materials tested in this present study, very few LAGBs were found. This is exemplified by the maps from the A15 and A25 samples in Fig. 5(b) and (c), respectively. All Al_2O_3-added materials showed very similar structures as A15 and A25, with very few LAGBs. From Fig. 5(a), (b) and (c), which share the same GROD colour scale, it can be seen that the overall intragranular (geometrically necessary) dislocation density, based on GROD values, is higher in A0 than in the Al_2O_3-added materials. As the samples were deformed to similar strains, and the intragranular dislocation density in the Al_2O_3-added materials was low, it is suggested that dislocation slip is not the dominating deformation mechanism in fine-grained Al_2O_3-added materials. However, the deformation was inhomogeneous, with some grains (typically grains with high Schmid factor for the $[11\bar{2}0](0001)$ slip system), were more deformed than other, often with GROD values increasing in specific crystallographic directions of the grain (perpendicular to [0001] direction), as previously observed in the coarse-grained Al_2O_3 material [16]. This suggests that even though dislocation slip is not the main deformation mechanism, it does occur in favourably oriented grains.

4. Discussion

Al_2O_3 was added to polycrystalline $Mo(Si,Al)_2$ with the intention to improve the high temperature mechanical properties. As expected, the Al_2O_3 particles had a grain boundary pinning effect during sintering, which rendered materials with finer microstructure than a Al_2O_3-free material. However, all fine-grained materials showed lower maximum stresses compared to the coarse-grained reference material when tested in compression at 1300 °C. This indicates that the deformation of $Mo(Si,Al)_2$-Al_2O_3 composites is very sensitive to grain size and that the deformation fine-grained materials is primarily controlled by creep mechanisms, such as grain boundary sliding or diffusion creep, rather than dislocation glide. The transition from dislocation glide to grain boundary sliding results in a decreasing strength with decreasing grain size, i.e. an inverse Hall–Petch relationship, for small grain sizes. This is supported by the results from the microstructural investigation, which showed that the fine-grained materials showed lower levels of internal misorientations (dislocation density) and had not, in contrast to coarse-grained Al_2O_3-free material, undergone (dislocation density-driven) DRX or formed LAGBs or highly deformed grains during deformation.

Even though the microstructures of the Al_2O_3-added materials were similar after deformation (apart from the different Al_2O_3 fractions), there was a large variation in maximum stress. This indicates that the Al_2O_3 fraction significantly affects the deformation response. Furthermore, the "U"-shaped trend of the maximum stress versus Al_2O_3 content (Fig. 4) suggests that competing mechanisms are active during compression. On the one hand, there is a softening mechanism which dominates at low Al_2O_3 levels (5–15 vol.%). On the other hand, at higher levels (20–25 vol.%), there is a gradual recovery of the strength. A similar trend, where two different mechanisms affect the strength of $MoSi_2$-based material, has been reported by Sadananda and Feng [18]. In Al-free $MoSi_2$, an amorphous SiO_2 film is present at the grain boundaries which makes the material very prone to creep and grain boundary sliding. It was shown that when adding C to the material, SiC was formed in an *in situ* reaction between C and the SiO_2 film. The formation of SiC particles had a grain size refining affect, which was detrimental for the creep resistance at elevated temperature (1200 °C). However, this was balanced by a decrease in creep tendency due to consumption of SiO_2 film. When compensated for the grain size, Sadananda and Feng did show that the particle strengthening had a positive effect on creep properties when the final volume fraction of SiC was higher than 20 vol.% [18]. This resembles the behaviour in our present study, even though the mechanisms are probably not the same as no amorphous film is present at the grain boundaries in $Mo(Si,Al)_2$. As discussed above, the lower stresses of the Al_2O_3 containing materials suggest that there is a strong effect of the grain size, and it is therefore probable that the strength recovery at higher fractions is related to the increased grain boundary strengthening effect from the added particles. However, the decreasing strength with increasing particle content at lower volume fractions (5–15 wt%) is harder to rationalize, as the grain size is approximately constant.

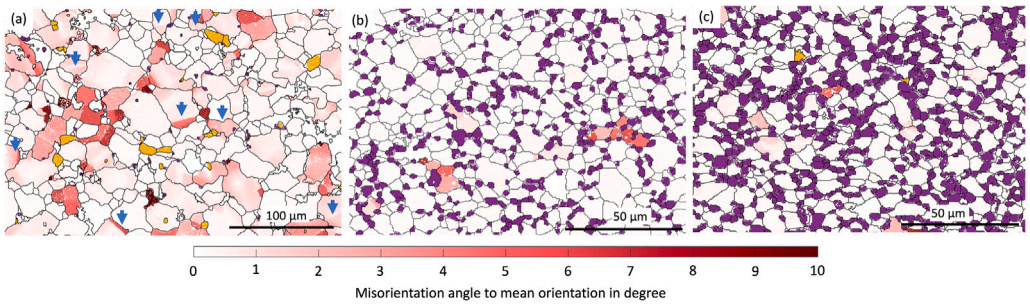

Fig. 5. (a) (b) and (c) show GROD maps of A0, A15 and A25, respectively. Arrows show low angle grain boundaries in (a). Violet regions are Al_2O_3 and yellow regions are $Mo_5(Si,Al)_3$. (For interpretation of the references to colour in this figure legend, the reader is referred to the web version of this article.)

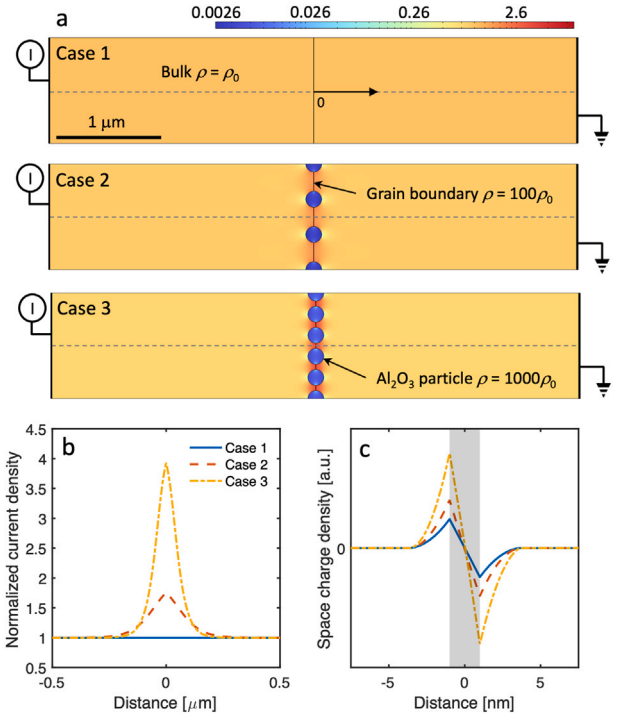

Fig. 6. Results of coupled thermo-electrical simulations. (a) Spatial current density distribution (logarithmic scale, normalized by the bulk value of case 1). (b) Current density (normalized by the bulk value) along the dashed lines in (a) for the different cases, showing a higher current density in the vicinity of the grain boundary, the effect increasing with decreasing particle spacing. (c) Space charge density in the grain boundary vicinity. The grey shaded area in (c) indicates the grain boundary.

It is possible that the "U"-shaped trend observed in Fig. 4 is related to the use of resistive heating. It is known that metals and ceramic materials often deform at lower stress levels when subjected to an electric current. This has been shown to be true even without a significant increase in temperature due to Joule heating, or when the increase in temperature has been corrected for in the analysis [28,29]. The phenomenon is referred *electroplasticity* and was first reported by Troitskii and Likhtman in 1963 [30], but is not yet fully understood. It has been argued that localized heating of grain boundaries contributes to the decrease in flow stress [31], and localized melting of grain boundaries has also been observed [32]. On the other hand, using simulations, Kim et al. [28] have shown that such localized heating is hard to explain due to rapid heat transfer from grain boundaries to grain interior. Instead, Kim et al. suggested that charge imbalance over grain boundaries is the main contributor to electroplasticity. It was argued that such imbalance should lead to weakening of atomic bonds, which could in turn promote grain boundary sliding. This was supported by first principle calculations showing an influence of charging on the optical phonon frequencies at grain boundaries [28]. Measurements of temperature compensated elastic modulus showed that the effect increases with decreasing grain size and increasing current density. Kim et al. further suggested that also the atomic diffusion rate might increase due to the charge imbalance. Campbell et al. [33] measured decreasing flow stress of polycrystalline Al_2O_3 in the presence of an electric field. This was attributed to a change in diffusion mechanism, from relatively slow lattice diffusion to faster diffusion at grain boundaries.

In the case of Al_2O_3-added $Mo(Si,Al)_2$, it is expected that the presence of particles with high electrical resistivity at the grain boundaries will increase the local current density by reducing the effective cross-section through which current is flowing. We qualitatively demonstrate this through simplified coupled thermo-electrical simulations using COMSOL Multiphysics 6.0 software. Three cases were investigated. Case 1 contained a single grain boundary, whereas cases 2 and 3 contained an increasing number of particles with high resistivity (simulating Al_2O_3 particles) at the boundary. The grain boundary was modelled as a 2 nm wide region with a resistivity $\rho_{gb} = 100\rho_0$, where ρ_0 is the bulk resistivity, while the resistivity of the particles was set to $\rho_p = 1000\rho_0$. Fig. 6 shows the resulting current density across the grain boundary for the different cases. We note that the presence of particles leads to a significant increase in the current density within some 250 nm from the boundary, which increases drastically as the spacing between particles is decreased (Fig. 6(b)). The increase is directly proportional to the reduction in area, as expected. We also note a very local increase in the space charge density in the vicinity of the boundary, which increases with decreasing particle spacing, that is, increasing the total particle volume. While this could support the charge imbalance mechanism proposed by Kim et al. [28], further detailed simulations are needed to draw any firm conclusions. Note that only time-independent (equilibrium) simulations were performed, so local Joule heating could not be observed.

Hence, independent of the actual mechanism(s) operating (local Joule heating, bond weakening or enhanced diffusion) an increased particle density is expected to lead to more pronounced electroplasticity through an increase in the local current density. This would explain the decreasing strength with increasing particle content in fine-grained $Mo(Si,Al)_2$ containing 5 to 15 wt% Al_2O_3. At higher Al_2O_3 contents (20 wt% or more) the particles act as obstacles which prevent grain boundary sliding as discussed above. This is in line with previous research on $MoSi_2$-SiC composites [18]. Therefore, we suggest that two competing mechanisms are active during deformation: (1) electroplasticity, which leads to a decrease in maximum stress, and (2) Al_2O_3 particle strengthening, which prevents grain boundary sliding and increases the maximum stress. At lower volume fractions the particle strengthening is not sufficient and the strength therefore decrease with increasing fraction. At a critical Al_2O_3 volume fraction, which in this study was around 15 wt% Al_2O_3, the particle strengthening become efficient enough to outweigh the electroplasticity-induced softening, and the strength increases with particle content. This is schematically shown in Fig. 7. The figure shows that the change in maximum stress

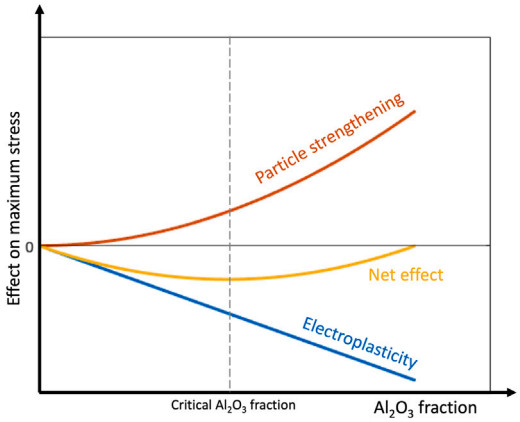

Fig. 7. Schematic illustration of the effect of electroplasticity and particle strengthening with increasing Al_2O_3 content.

is negative when considering the electroplastic effect on its own, and positive when considering only the particle strengthening effect. The net effect of the two mechanisms results in a convex function, having a minima at the critical Al_2O_3 fraction.

Electroplasticity is particularly important since the application of these materials is resistive heating. The possible electroplasticity effects will therefore always be present and should be accounted for, e.g. if using strength values determined by tests with external heating in the stress calculations and design. In order to confirm that the decrease in maximum stress observed in this study is influenced by electroplasticity, additional experiments need to be conducted using an alternative (external) heating system. Indeed, if the proposed explanation for the "U"-shaped curve is correct, the absence of current-induced electroplasticity would allow particle strengthening to operate already from the lowest particle fractions. This would lead to a continuously increasing strength (at constant grain size) and suggests that particle strengthening could still prove to be a valid strengthening mechanism for applications other than resistive heating elements. Furthermore, dedicated experiments to separate the effects of particle fraction and grain size are also needed, and will help elucidate the underlying deformation mechanisms of $Mo(Si,Al)_2$-based materials.

On a final note, considering the increasing strength levels at larger particle fractions it would be interesting to investigate if this trend continues to even higher Al_2O_3 contents. This could ultimately result in strength levels higher than A5 (i.e. at constant grain size), and perhaps even A0. However, a higher volume fraction of Al_2O_3 particles might pose challenges for electrical heating. Furthermore, it is likely that the oxidation resistance of the material will be negatively affected by a higher Al_2O_3 content, if continuous networks are formed.

5. Summary

- The maximum stress of polycrystalline $Mo(Si,Al)_2$ is sensitive to grain size. Fine-grained materials deform plastically at lower stresses than a coarse-grained material, suggesting that creep-like mechanisms dominate under the current test conditions (1300 °C and a nominal strain rate of 10^{-4} s^{-1}).
- Contrary to the coarse-grained Al_2O_3-free reference, no grain refinement through DRX occurred in the fine-grained materials, and very few LAGBs could be observed. Furthermore, the internal misorientation gradients were small in the deformed state. This supports the suggestion that diffusion dependent creep mechanisms dominate, rather than intragranular dislocation motion.
- We observe a complex Al_2O_3 particle fraction dependence of the strength, where an increased fraction initially leads to a decrease in the maximum stress. A minimum is reached around 15 wt%, after which the strength gradually recovers with increasing fractions. We suggest that this is an effect of the resistive heating mode, leading to the occurrence of electroplasticity, which reduces the strength with increasing fraction. This is counteracted by grain boundary strengthening, which increases with increasing fraction. Electroplasticity dominates at lower fractions, whereas at higher fractions the particle strengthening takes over. This also suggests that in the absence of current-induced electroplasticity Al_2O_3 additions would lead to a continuous strength increase with volume fraction at constant grain size.

CRediT authorship contribution statement

Aina Edgren: Conceptualization, Methodology, Investigation, Writing – original draft, Visualization. **Erik Ström:** Supervision, Conceptualization, Resources, Writing – review & editing. **Lars Frisk:** Investigation, Resources. **Farid Akhtar:** Investigation, Resources, Writing – review & editing. **Magnus Hörnqvist Colliander:** Supervision, Conceptualization, Writing – review & editing, Funding acquisition, Project administration.

Declaration of competing interest

The authors declare the following financial interests/personal relationships which may be considered as potential competing interests: Aina Edgren and Erik Ström are employees of Kanthal AB, a manufacturer of commercial heating elements.

Data availability

Data will be made available on request.

Acknowledgements

This research was funded by the Swedish Foundation for Strategic Research (SSF), Sweden and Kanthal AB, Sweden, through the industrial Ph.D. student grant ID18-0064. The work was performed in part at Chalmers Materials Analysis Laboratory (CMAL).

Appendix A. Supplementary data

Supplementary material related to this article can be found online at https://doi.org/10.1016/j.msea.2023.144583.

References

[1] H. Ritchie, M. Roser, P. Rosado, CO_2 and greenhouse gas emissions, Our World Data (2020) https://ourworldindata.org/co2-and-other-greenhouse-gas-emissions. Accessed: 2022-10-14.
[2] S. Madeddu, F. Ueckerdt, M. Pehl, J. Peterseim, M. Lord, K.A. Kumar, C. Krüger, G. Luderer, The CO_2 reduction potential for the European industry via direct electrification of heat supply (power-to-heat), Environ. Res. Lett. 15 (12) (2020) 124004.
[3] Sandvik Materials Technology, Kanthal super electric heating elements, 2012, https://www.kanthal.com/globalassets/kanthal-global/downloads/furnace-products-and-heating-systems/heating-elements/mosi2-heating-elements/s-ka058-b-eng-2012-01.pdf Accessed: 2021-11-13.
[4] M. Halvarsson, T. Jonsson, L. Ingemarsson, M. Sundberg, J.E. Svensson, L.G. Johansson, Microstructural investigation of the initial oxidation at 1450 °C and 1500 °C of a $Mo(Si,Al)_2$-based composite, Mater. High Temp. 26 (2) (2009) 137–143.
[5] L. Ingemarsson, M. Halvarsson, J. Engkvist, T. Jonsson, K. Hellström, L.G. Johansson, J.E. Svensson, Oxidation behavior of a $Mo(Si,Al)_2$-based composite at 300-1000 °C, Intermetallics 18 (2010) 633–640.
[6] L. Ingemarsson, K. Hellström, L.G. Johansson, J.E. Svensson, M. Halvarsson, Oxidation behaviour of a $Mo(Si,Al)_2$ based composite at 1500 °C, Intermetallics 19 (9) (2011) 1319–1329.
[7] L. Ingemarsson, K. Hellström, S. Canovic, T. Jonsson, M. Halvarsson, L.G. Johansson, J.E. Svensson, Oxidation behavior of a $Mo(Si,Al)_2$ composite at 900-1600 °C in dry air, J. Mater. Sci. 48 (4) (2013) 1511–1523.

[8] K. Yanagihara, T. Maruyama, K. Nagata, High temperature oxidation of Mo-Si-X intermetallics (X=Al, Ti, Ta, Zr and Y), Intermetallics 3 (3) (1995) 243–251.
[9] R. Mitra, V.V. Rama Rao, Effect of minor alloying with Al on oxidation behaviour of $MoSi_2$ at 1200 °C, Mater. Sci. Eng. A 260 (1–2) (1999) 146–160.
[10] A. Edgren, L.G. Johansson, E. Ström, M. Hörnqvist Colliander, Influence of yttrium doping on the oxidation of $Mo(Si,Al)_2$ in air at 1500 °C, Oxid. Met. (0123456789) (2022).
[11] H. Inui, M. Moriwaki, K. Ito, M. Yamaguchi, Plastic deformation of single crystals of $Mo(Si,Al)_2$ with the C40 structure, Philos. Mag. A 77 (2) (1998) 375–394.
[12] K. Hagihara, T. Nakano, Y. Umakoshi, Mechanical properties of C40-based ternary $Mo(Si,Al)_2$ and quaternary $(Mo,Zr)(Si,Al)_2$ silicides, Scr. Mater. 38 (3) (1998) 471–476.
[13] Y. Umakoshi, T. Nakano, K. Kishimoto, D. Furuta, K. Hagihara, M. Azuma, Strength and deformation mechanism of C40-based single crystal and polycrystalline silicides, Mater. Sci. Eng. A 261 (1–2) (1999) 113–121.
[14] K. Niihara, Y. Suzuki, Strong monolithic and composite $MoSi_2$ materials by nanostructure design, Mater. Sci. Eng. A 261 (1–2) (1999) 6–15.
[15] Y. Suzuki, A. Nakahira, T. Sekino, K. Niihara, Microstructure and mechanical properties of Mo-Si-Al alloy and Mo-Si-Al/SiC composite, J. Jpn. Soc. Powder Powder Metal. 43 (3) (1996) 272–277.
[16] A. Edgren, E. Ström, R. Qiu, L. Frisk, F. Akhtar, M.H. Colliander, High temperature deformation of polycrystalline C40 $Mo(Si,Al)_2$, Mater. Sci. Eng. A 849 (2022) 143387.
[17] A. Newman, S. Sampath, H. Herman, Processing and properties of $MoSi_2$-SiC and $MoSi_2$-Al_2O_3, Mater. Sci. Eng. A 261 (1) (1999) 252–260.
[18] K. Sadananda, C.R. Feng, Effect of carbon addition on the creep of molybdenum disilicide composites, Mater. Sci. Eng. A 192–193 (PART 2) (1995) 862–867.
[19] R.M. Aikin, Strengthening of discontinuously reinforced $MoSi_2$ composites at high temperatures, Mater. Sci. Eng. A 155 (1–2) (1992) 121–133.
[20] A. Basu, A. Ghosh, The effect of deformation and reinforcement particles on the grain growth behavior of $MoSi_2$, MRS Proc. 322 (1993) 41.
[21] S.A. Maloy, J.J. Lewandowski, A. Heuer, J.J. Petrovic, Effects of carbon additions on the high temperature mechanical properties of molybdenum disilicide, Mater. Sci. Eng. A 155 (1992) 159–163.
[22] S. Maloy, A.H. Heuer, J. Lewandowski, J. Petrovic, Carbon additions to molybdenum disilicide: Improved high-temperature mechanical properties, J. Am. Ceram. Soc. 74 (10) (1991) 2704–2706.
[23] R. Li, B. Li, X. Chen, J. Wang, T. Wang, Y. Gong, S. Ren, G. Zhang, Variation of phase composition of Mo-Si-B alloys induced by boron and their mechanical properties and oxidation resistance, Mater. Sci. Eng. A 749 (2019) 196–209.
[24] R. Aikin Jr., Strengthening of discontinuously reinforced $MoSi_2$ composites at high temperatures, Mater. Sci. Eng. A 155 (1992) 121–133.
[25] M. Esmaeili Ghayoumabadi, A. Saidi, M.H. Abbasi, Lattice variations and phase evolutions during combustion reactions in Mo-Si-Al system, J. Alloys Compd. 472 (1–2) (2009) 84–90.
[26] F. Bachmann, R. Hielscher, H. Schaeben, Texture analysis with MTEX- free and open source software toolbox, Solid State Phenomena 160 (2010) 63–68.
[27] J.D. French, S.M. Wiederhorn, H.J. Petrocic, Creep rupture of $MoSi_2/SiC_p$ composites, in: Materials Research Society Symposium Proceedings, 1994, p. 203.
[28] M.J. Kim, S. Yoon, S. Park, H.J. Jeong, J.W. Park, K. Kim, J. Jo, T. Heo, S.T. Hong, S.H. Cho, Y.K. Kwon, I.S. Choi, M. Kim, H.N. Han, Elucidating the origin of electroplasticity in metallic materials, Appl. Mater. Today 21 (2020) 100874.
[29] H. Conrad, D.I. Yang, Influence of an Electric Field on the Plastic Deformation of Fine-Grained MgO at High Homologous Temperatures, Technical Report, 2000, pp. 4045–4052.
[30] O.A. Troitskii, V.I. Likhtman, The anisotropy of the action of electron and γ radiation on the deformation of zinc single crystals in the brittle state, Sov. Phys. Dokl. 8 (1963) 91.
[31] J. Zhao, Relating Grain Boundaries to the Mechanical Properties of Polycrystalline Material: Gradient Nanocrystalline Material and Electro-Plasticity (Ph.D. thesis), University of Akron, 2018.
[32] R. Fan, J. Magargee, P. Hu, J. Cao, Influence of grain size and grain boundaries on the thermal and mechanical behavior of 70/30 brass under electrically-assisted deformation, Mater. Sci. Eng. A 574 (2013) 218–225.
[33] J. Campbell, Y. Fahmy, H. Conrad, Influence of an electric field on the plastic deformation of fine-grained Al_2O_3, Metall. Mater. Trans. A 30 (11) (1999) 2817–2823.